Soft Matter

Diverse balances of tubulin interactions and shape change drive and interrupt microtubule depolymerization

Journal:	*Soft Matter*
Manuscript ID	SM-ART-07-2019-001323.R1
Article Type:	Paper
Date Submitted by the Author:	09-Sep-2019
Complete List of Authors:	Bollinger, Jonathan; Sandia National Laboratories, Center for Integrated Nanotechnologies Stevens, Mark; Sandia National Laboratories, Center for Integrated Nanotechnologies

Journal Name

ARTICLE TYPE

Cite this: DOI: 10.1039/xxxxxxxxxx

Diverse balances of tubulin interactions and shape change drive and interrupt microtubule depolymerization†

Jonathan A. Bollinger[a] and Mark J. Stevens*[a]

Received Date
Accepted Date

DOI: 10.1039/xxxxxxxxxx

www.rsc.org/journalname

Microtubules are stiff biopolymers that self-assemble via the addition of GTP-tubulin ($\alpha\beta$-dimer bound to GTP), but hydrolysis of GTP- to GDP-tubulin within the tubules destabilizes them toward catastrophically-fast depolymerization. The molecular mechanisms and features of the individual tubulin proteins that drive such behavior are still not well-understood. Using molecular dynamics simulations of whole microtubules built from a coarse-grained model of tubulin, we demonstrate how conformational shape changes (i.e., deformations) in subunits that frustrate tubulin-tubulin binding within microtubules drive depolymerization of stiff tubules via unpeeling "ram's horns" consistent with experiments. We calculate the sensitivity of these behaviors to the length scales and strengths of binding attractions and varying degrees of binding frustration driven by subunit shape change, and demonstrate that the dynamic instability and mechanical properties of microtubules can be produced based on either balanced or imbalanced strengths of lateral and vertical binding attractions. Finally, we show how catastrophic depolymerization can be interrupted by small regions of the microtubule containing undeformed dimers, corresponding to incomplete lattice hydrolysis. The results demonstrate a mechanism by which microtubule rescue can occur.

1 Introduction

Microtubules (MTs) are biopolymers critical for cellular function and relevant for diverse engineering applications due to their rich mechanical and dynamic behaviors. Their roles as cytoskeletal components, drivers of mitosis, and tracks for motor proteins derive from their self-assembly into highly stiff, high aspect ratio hollow fibers (composed solely of $\alpha\beta$-tubulin dimers) that exhibit a distinctive *dynamic instability*.[1,2] While polymerization proceeds slowly via the addition of GTP-tubulin dimers (tubulin bound to GTP), hydrolysis of GTP- to GDP-tubulin away from the leading GTP-tubulin "cap" eventually destabilizes tubules toward catastrophically-fast depolymerization once the cap disappears.[2,3] This depolymerization, during which the MT unpeels with outwardly-curving "ram's horns", produces work and leads to dissociation of GDP-tubulin, which can be recycled into new tubules (if re-converted to GTP-tubulin).[4–8] In addition, depolymerizing MTs can also undergo "rescue", wherein depolymerization is halted in-progress and growth recommences.[2] The emergence of such complex and important functions from one protein building block (with two nucleotide states) has made MTs attractive targets for cancer disruption[9] and models for biology-inspired responsive materials, including synthetic tubules,[10] switchable gels and films,[11] and active (i.e., driven) liquid-crystal systems.[12] But to design for such applications, it is critical to better understand the molecular origins and features of the individual tubulin dimers that drive the dynamic instability and rescue.

Experimental characterization and computer modeling support the long-standing hypothesis that the dynamic instability emerges due to subunit *shape change* (i.e., allosteric deformation) of tubulin in response to lattice hydrolysis, but questions still remain about the nature of such a conformational switch.[4,8,13–15] For example, recent experiments[16,17] show how hydrolysis is associated with a shape change in tubulin from a "straight" conformation compatible with lattice binding and polymerization to a "bent" conformation commensurate with the curvature of GDP-tubulin protofilaments observed during depolymerization.[13,18,19] More specifically, this shape change appears to be a localized *compression* of the outwardly-facing domains of the α-subunit (with β-subunits unaffected in terms of shape) that frustrates tubulin-tubulin binding and, across many hydrolysis events, generates collective stress capable of driving depolymerization.[16,17] Mean-

[a] *Center for Integrated Nanotechnologies, Sandia National Laboratories, Albuquerque NM 87185, USA*
* *E-mail: msteve@sandia.gov*
† Electronic Supplementary Information (ESI) available: Movies of microtubule simulations. See DOI: 10.1039/b000000x/

while, computer modeling of MTs has not only captured the corresponding kinetics of growth and depolymerization at various levels of detail, but also how hydrolysis-induced changes in tubulin binding that favor curved protofilaments can facilitate depolymerization.[20–28] From a molecular perspective, our own previous modeling study demonstrates explicitly how α-subunit compression resembling that observed via cryo-EM is sufficient to yield stiff tubules exhibiting a dynamic instability.[29] Together, these studies point to shape change as necessary and (likely) sufficient ingredient for driving depolymerization, but basic questions remain, including: How sensitive is the emergence of the dynamic instability to the degree of tubulin shape change? How do the ranges and strengths of tubulin-tubulin binding attractions modulate the structural-dynamic impacts of tubulin shape change? And how are collective properties like MT stiffness affected by these factors?

In tandem with these studies implicating tubulin shape change as a driving force for depolymerization, other experiments have demonstrated that unhydrolyzed— or, by extension, undeformed— tubulin dimers may correspondingly interrupt depolymerization, though there has been limited testing of this hypothesis via, e.g., computer modeling. Here, it has been thought for some time that unhydrolyzed GTP-tubulin dimers may be the cause of stochastic interruptions to depolymerization in progress, therefore serving as potential points for MT rescue.[30] Dimitrov et. al. have provided a demonstration of this concept by using antibody labeling to identify unhydrolyzed regions of MT lattices, showing correspondence between GTP-tubulin—rich regions (i.e., so-called "GTP remnants") and rescue locations.[31] In turn, more recent work on MTs comprised of alternating regions of hydrolyzed and unhydrolyzed dimers has shown systematic slowdown of depolymerization and/or promotion of rescue in regions containing unhydrolyzed tubulin.[32–34] However, while these studies support the idea that lattice regions containing unhydrolyzed dimers can interrupt and reverse depolymerization, they do not explicitly address the specific local nature of any underlying (lack of) shape change. Likewise, while modeling studies have captured rescue events in the kinetic sense,[26,35] there has been little systematic investigation from a three-dimensional micro-mechanical perspective of how depolymerization might be interrupted or reversed on the basis of tubulin dimer shape. This leaves open questions related to those above: Can depolymerization indeed be interrupted *in-progress* due to the presence of dimers that have not undergone shape change? If so, what regions of these dimers— in terms of size, shape, and composition— are sufficient to interrupt depolymerization such that growth can reinitiate?

To address these knowledge gaps, we perform molecular dynamics (MD) simulations of whole MTs built from a coarse-grained model of tubulin to show how catastrophic depolymerization, rescue, and other properties such as tubule mechanical stiffness emerge due to subunit shape change (or lack thereof). We begin by reporting the structural dynamics of capped and uncapped model MTs as a function of the length scale of tubulin-tubulin attractions, the degree of tubulin deformation (i.e., α-subunit compression) and the strengths of lateral and vertical binding attractions. Within this four-dimensional parameter space that characterizes our systems, we find the sub-space or *manifold* of parameter combinations corresponding to dynamic instability, where this manifold comprises: (1) modest compressions of α-subunits, consistent with known tubulin conformations, that frustrate binding of attraction sites between neighboring lattice dimers and (2) narrow ranges of tubulin-tubulin binding enthalpies that balance emergence of and stabilization against lattice strain of capped MTs with the requirement that dimers dissociate from ends of ram's horn during depolymerization of uncapped MTs. Notably, we observe that *diverse* ratios of lateral- versus vertically-biased tubulin-tubulin attractions can work in concert with subunit shape change to facilitate depolymerization of otherwise stiff tubules. We also characterize how shifting the length scales and balances of attractions can impact tubule persistence length, depolymerization rate, and the length of ram's horns. Finally, we demonstrate that small patchy regions of only two or three dozen uncompressed dimers can indeed interrupt catastrophic depolymerization in-progress for timescales that are commensurate with MT (re-)growth, in line with the picture of "GTP remnants" as points for rescue initiation in experiments.

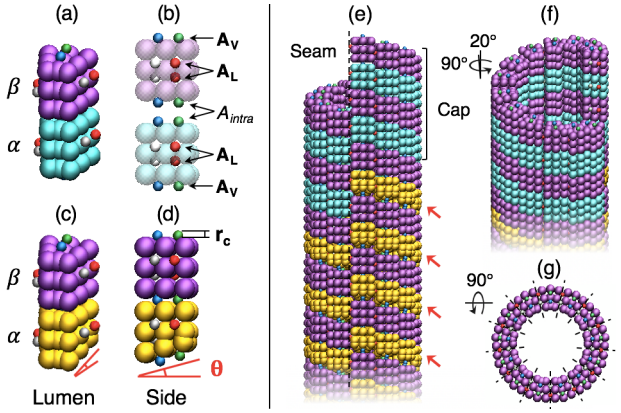

Fig. 1 (a-d) Coarse-grained dimer model of $\alpha\beta$-tubulin comprising wedge-shaped β-subunits (purple) bound to α-subunits that are (a,b) identical in shape to β-subunits (cyan) or (c,d) compressed with angle θ (gold). Subunits are effectively rigid and comprise 27 purely-repulsive beads and 8 attractive sites, including four vertical-binding (V) beads (pairs of blue, green) and four lateral-binding (L) beads (pairs of white, red). Attractive sites have color-specific interactions, with lateral sites offset vertically to favor the chiral MT lattice. As highlighted in (b), pairs of vertical (lateral) attractive sites on the exposed dimer sides are parameterized by attraction strengths A_V (A_L), while intra-dimer vertical beads are parameterized via A_{intra}. As highlighted in (d), ranges of attractive beads are set by cutoff r_c. (e-g) Model dimers assembled into a capped GDP-MT populated with compressed α-subunits except within terminal region of uncompressed dimers. As shown in (g), wedges are shaped so that 13 vertical protofilaments (demarcated by dashed lines) fit in the MT lattice. Rotations listed in (f,g) are relative to the view in (e).

2 Methods

We consider a previously-described[29] coarse-grained model of $\alpha\beta$-tubulin suitable for simulating whole MTs. As shown in Fig. 1, α- and β-subunits are represented by wedges decorated with short-range attractive sites to represent tubulin–tubulin binding regions, a motif derived from earlier tubule-forming wedge particles.[36,37] The wedges themselves are composites of 27 purely-

repulsive beads that interact with the analogous beads of other wedges via the cut and shifted Lennard Jones pair potential $U_{\rm LJ}(r) = 4\epsilon[(\sigma/r)^{12} - (\sigma/r)^6] + \epsilon$ out to cutoff distance of $2^{1/6}\sigma$, where ϵ is the characteristic energy scale and σ is the bead diameter. (Below, we assume an approximate conversion $\sigma \approx 1.5$nm when working in real length units.) These wedge beads are situated such that their excluded volume allows for 13 wedges (or protofilaments) to make a complete ring. In turn, each wedge has eight attractive sites divided into two lateral and two vertical pairs, where lateral pairs of sites are vertically offset such that when subunits are in register, they are situated in the pitch-3 chiral lattice of MTs. Attractive sites interact with their counterparts on the *opposite* (i.e., top-to-bottom, left-to-right, etc.) surface of a neighboring wedge via the pair potential $U_{\rm A}(r) = -A[1 + \cos(\pi r/r_c)]$ out to attraction cutoff $r_{\rm c}$, where the prefactors A for lateral and vertical attractive sites are denoted $A_{\rm L}$ and $A_{\rm V}$, respectively. We define the characteristic maximum dimer binding enthalpy given two dimer neighbors (one lateral and one vertical) as

$$\Delta H_{\rm D}^{\rm max} = \Delta H_{\rm D,L}^{\rm max} + \Delta H_{\rm D,V}^{\rm max} = 8A_{\rm L} + 4A_{\rm V} \quad (1)$$

which accounts for the multiple sites involved in dimer-dimer binding and for the well depth of the potential $U_{\rm A}(r) = 2A$. Throughout the text, we refer to interactions as "laterally-biased" when $\Delta H_{\rm D,L}^{\rm max} > \Delta H_{\rm D,V}^{\rm max}$ (i.e., $A_{\rm L} > 0.5A_{\rm V}$) and "vertically-biased" when $\Delta H_{\rm D,L}^{\rm max} < \Delta H_{\rm D,V}^{\rm max}$ (i.e., $A_{\rm L} < 0.5A_{\rm V}$). While we vary the attraction strengths $A_{\rm L}$ and $A_{\rm V}$ between subunits of neighboring dimers throughout the study, we fix the vertical interactions between α and β subunits of the same dimer (i.e., intra-dimer attractions) at $A_{intra} = 8.0k_{\rm B}T$ across all cases to prevent self-dissociation.

The $\alpha\beta$-tubulin dimers prior to MT hydrolysis (i.e., lattice composed of GTP-tubulin) are represented with two identical wedge monomers (Figs. 1(a–b)), while $\alpha\beta$-tubulin dimers after MT hydrolysis (i.e., lattice composed of GDP-tubulin) are represented by replacing the α-subunit wedge with one that has been *compressed* by angle θ (Figs. 1(c–d)) in the vertical direction to approximate the hydrolysis-driven conformational effects observed in experiments.[16] Due to the placement of binding sites, the *uncompressed* dimers energetically favor straight protofilaments, while the *compressed* dimers favor curved protofilaments and exhibit frustrated lateral versus vertical binding when protofilaments are bound together in a lattice. In our former study,[29] we fixed $\theta = 15°$ to roughly mimic the relative rotation of subunits in bent tubulin compared to straight tubulin;[13,18] however, in this study, we consider $\theta = 10°$, $15°$, and $20°$. Given these θ values, our curved protofilaments respectively have radii of curvature $R \approx 46.5$nm, 28nm, and 21nm, respectively, where the middle of this range is comparable to experimental measurements for GDP-tubulin protofilaments.[13,19]

We characterize model MT structural dynamics as a function of $r_{\rm c}$, θ, $A_{\rm L}$, and $A_{\rm V}$ by pre-building tubules out of these two types of dimers. Broadly, we consider three classes of model MTs: (1) capped GDP-MTs (illustrated in Figs. 1(e–g)), which are comprised of compressed dimers except for the two (or three, if noted) terminal plus-end rows that are populated with uncompressed dimers, representing a small GTP-rich region; (2) uncapped GDP-MTs, which are solely comprised of compressed dimers; and (3) GTP-MTs, which are comprised solely of uncompressed dimers. To test for the interruption of depolymerization, we also consider uncapped GDP-MTs that have small mid-lattice regions partially-populated with uncompressed dimers. In all cases examined here, we model all MTs in isolation and specifically consider GDP-MTs after hydrolysis of the tubule lattice from GTP- to GDP-tubulin, while not modeling individual hydrolysis events. The minus ends of all model MTs are stabilized to prevent drift by assigning two dimer rows with uncompressed α-subunits that are tethered to their initial positions. Unless otherwise noted, we simulate tubules that are 40 dimer rows long (equivalent to 360nm).

We perform MD simulations using LAMMPS[38] with time-step $\delta t = 0.005\tau$, where $\tau = \sigma(m/\epsilon)^{1/2}$ and m is the reference mass of one bead. Temperature is fixed via a Langevin thermostat (damping constant $1.0\tau^{-1}$) at $T = 1.0\epsilon/k_{\rm B}$, where $k_{\rm B}$ is Boltzmann's constant (this sets the characteristic energy scale as $k_{\rm B}T$). The wedge subunits (including attractive sites) are effectively treated as rigid bodies, with all beads connected to their neighbors via harmonic potentials with spring constant $K = 500k_{\rm B}T/\sigma^2$.

For select parameters sets, we also measure persistence lengths $\ell_{\rm p}$ via separate simulations that mimic passive MT deflection experiments.[39] As described previously,[29] we simulate GTP-MTs (to represent Taxol-stablized MTs[16]) and capped GDP-MTs using the protocols above, except that we increase the Langevin damping constant to $100.0\tau^{-1}$ to lower the effective viscosity of the implicit solvent and improve sampling of the equilibrium deflections of the whole model MTs. In turn, we calculate the lateral deflection x between the centers of mass of the top row (fluctuating) and bottom row (tethered to prevent drift). Based on the probability distribution of deflections, we then calculate $\ell_{\rm p} = L^3/(3\langle\Delta x^2\rangle)$ where L is the average model MT contour length and $\langle\Delta x^2\rangle$ is the (Gaussian) variance of the MT deflection x.

3 Results & Discussion

3.1 Structural dynamics

Fig. 2 shows the categories of structural dynamics that we observe for the model GDP-MTs as a function of attraction cutoff $r_{\rm c}$ (fixed in Fig. 2), compression angle θ and attraction strengths $A_{\rm L}$ and $A_{\rm V}$— including the target MT dynamic instability. In line with our previous work,[29] we broadly divide structural dynamics into those cases where capped GDP-MTs are either *unstable* or *stable*— the latter a necessary feature of the dynamic instability. To test for stability, we simulate capped GDP-MTs up to 160 dimers long (1.4μm) for time scales of at least $5\text{x}10^6\tau$ to confirm that they exhibit no spontaneous failures. Failures include *cap loss*, where interactions are so weak that caps immediately dissolve; *cap splits*, where strong vertical interactions force immediate outward curling of all protofilaments regardless of stabilization; and *lattice splits* that develop due to internal destabilizing modes. Any instances of these behaviors are categorized as *unstable*. In contrast, for all conditions where capped GDP-MTs are *stable*, we then determine the corresponding structural dynamics in the absence of a

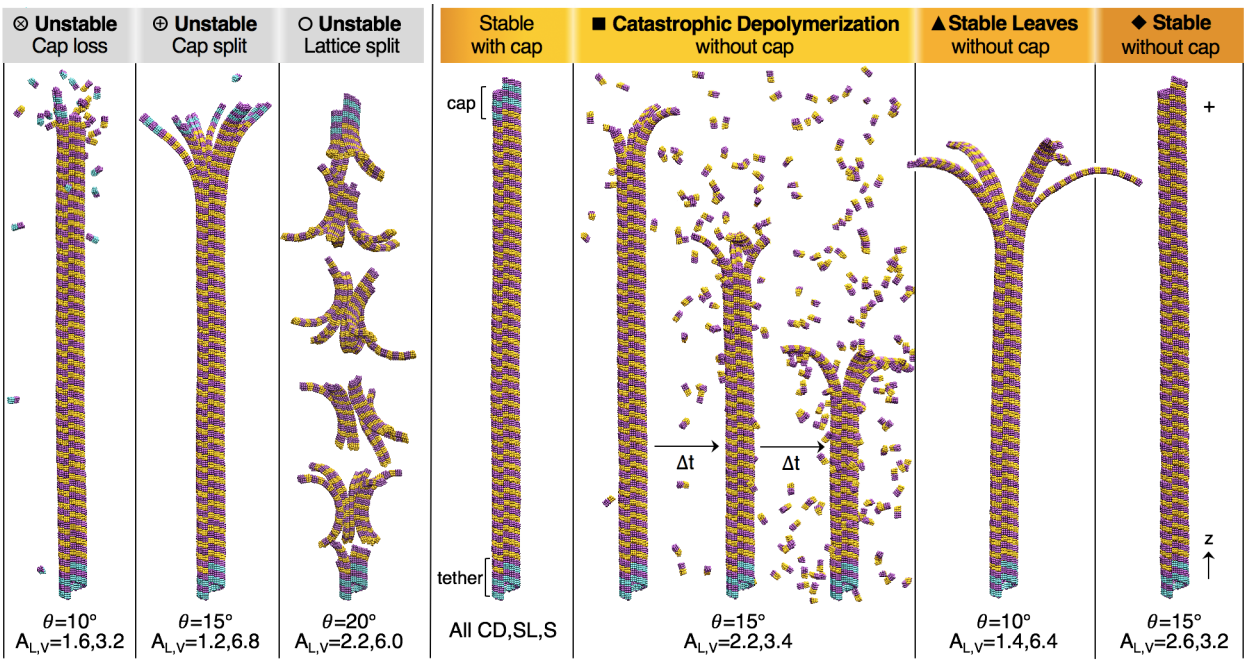

Fig. 2 Categories of GDP-MT behavior observed for various parameter combinations of attraction cutoff r_c, compression angle θ and lateral (A_L) and vertical (A_V) attraction strengths. In this figure, $r_c = 0.50\sigma$ in all cases and attraction strengths are listed in units of k_BT. Point types in header are used in subsequent figures. Snapshots are from MD simulations of GDP-MTs initially 40 dimer rows long (i.e., 360nm) with minus ends tethered to prevent drift. Parameter combinations corresponding to *unstable* conditions include cases where capped GDP-MTs (caps comprising 2 terminal rows of uncompressed dimers) exhibit rapid *cap loss* (x-circle) or immediate *cap split(s)* (+-circle) that expose GDP-MT lattices prone to fracture and/or depolymerization, or alternatively where caps are highly stable but tubules exhibit spontaneous *lattice split(s)* (unfilled circle) leading to disassembly. For all other categories, GDP-MTs are stable when capped (see text), but when uncapped either undergo *catastrophic depolymerization* (CD, filled square) while releasing dimers from unpeeling "ram's horns" (shown as time-lapse series with $\Delta t = 7.5x10^5\tau$); unpeel without commensurate dimer loss, resulting in *stable leaves* (SL, filled triangle); or remain perpetually *stable* (S, filled diamond). Symbols corresponding to behavior categories are used in Figs. 3 and 4.

cap, observing either: *catastrophic depolymerization*, where GDP-MTs unpeel from their plus ends and steadily release dimers from ram's horns that resemble those in cryo-EM images of depolymerizing MTs;[4,8] *stable leaves*, where GDP-MTs unpeel from their plus ends while releasing very few dimers, eventually forming permanent ram's horns of stable length; or *stable* MTs that exhibit no unpeeling and virtually no plus-end dissociation. Following our previous work,[29] we also confirm that for all conditions where GDP-MTs exhibit catastrophic depolymerization, stable leaves, or stablity in the absence of a cap, that GTP-MTs with the same r_c, A_L, and A_V are stable, which isolates the shape frustration as the cause of the structural dynamics.

Fig. 3 shows how these types of structural dynamics emerge relative to one another for fixed $r_c = 0.50\sigma$, highlighting how catastrophic depolymerization occurs along a narrow manifold within the available parameter space where interactions must simultaneously be strong in some respects, but weak in others. Specifically, the dimer interactions must be strong enough to provide mechanical stability of the MT lattice prior to depolymerization and strong enough for geometric frustration to produce destabilizing strain when uncapped, yet weak enough for dimers to dissociate from exposed ram's horns once depolymerization is in progress. For example, the middle panel of Fig. 3 expands on our previous findings[29] that focused on $\theta = 15°$, where catastrophic depolymerization conditions occur for a small window of attraction strengths bounded by regions where GDP-MT lattices and/or caps are either unstable due to weak and unbalanced attractions, or alternatively where little to no dimer dissociation can occur due to overly-strong attractions (thereby preventing depolymerization). The left panel shows how lowering the compression angle to $\theta = 10°$ shifts the catastrophic depolymerization regime toward combinations of attraction strengths that are more vertically-biased (e.g., $A_{L,V} = 1.4,4.8k_BT$), which increases the effect of the relatively diminished geometric frustration. In turn, catastrophic depolymerization conditions still lie at the boundary of lattice and/or cap instability. Though this boundary can be moved slightly left toward smaller attraction strengths by increasing the size of the cap from two to three rows, which circumvents cap splits, it is also clear that for our "standard minimum" cap comprising two rows, the catastrophic depolymerization region has narrowed relative to the $\theta = 15°$ case. Finally, the right panel for $\theta = 20°$ demonstrates that there is a finite tolerance for generating catastrophic depolymerization with respect to increasing amounts of geometric frustration: in essence, for $\theta = 20°$ and above, stabilizing GDP-MT lattices against spontaneous mid-tubule lattice splits requires such high binding strengths that dissociation of dimers is virtually impossible even if GDP-MTs do unpeel when uncapped.

Altogether, Fig. 3 suggests that for fixed r_c, the catastrophic depolymerization manifold spans the intersection of (1) a small but finite range of θ-values and (2) A_L and A_V strengths that combine to give a maximum dimer binding enthalpy of approximately

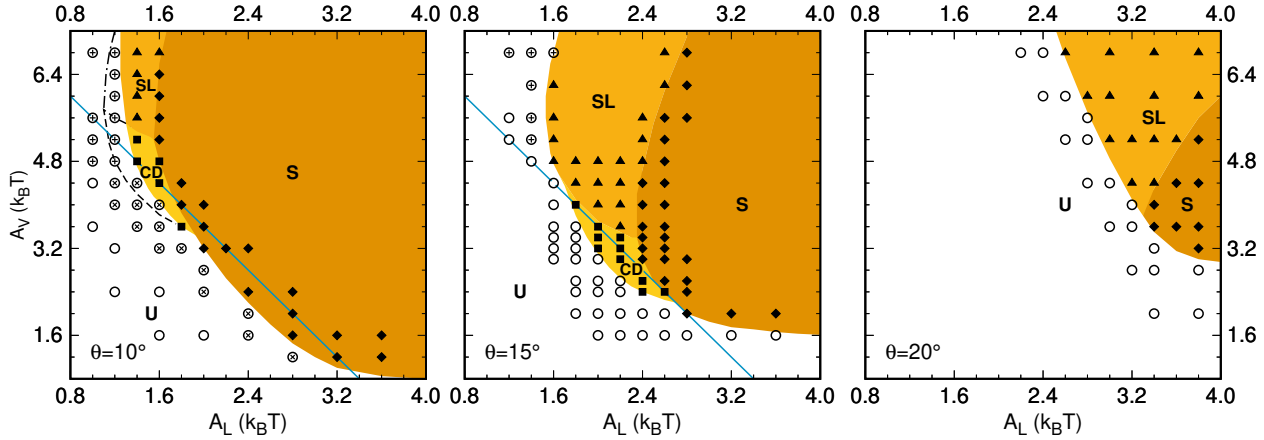

Fig. 3 GDP-MT behaviors as a function of vertical (A_V) and lateral (A_L) attraction strengths for $r_c = 0.50\sigma$ and $\theta = 10°$ (left), $15°$ (middle), or $20°$ (right). Filled symbols denote where GDP-MTs are stable given 2-row caps while uncapped GDP-MTs exhibit catastrophic depolymerization (CD, squares), stable leaves (SL, triangles), or stability (S, diamonds). Unfilled symbols denote where GDP-MTs with 2-row caps are unstable (U), undergoing either cap loss (x-circles), cap fracture (+-circles), or lattice fracture(s) (unfilled circles). Symbols correspond to the snapshots in Fig. 2. Unstable points located to the right of dashed (dot-dashed) borders denote where GDP-MTs with 3-row caps are stable while uncapped GDP-MTs exhibit catastrophic depolymerization (stable leaves). Solid blue lines in left and middle panels trace parameter sets where $\Delta H_D^{max} \approx 30.4 k_B T$, which intersect with CD conditions (see text).

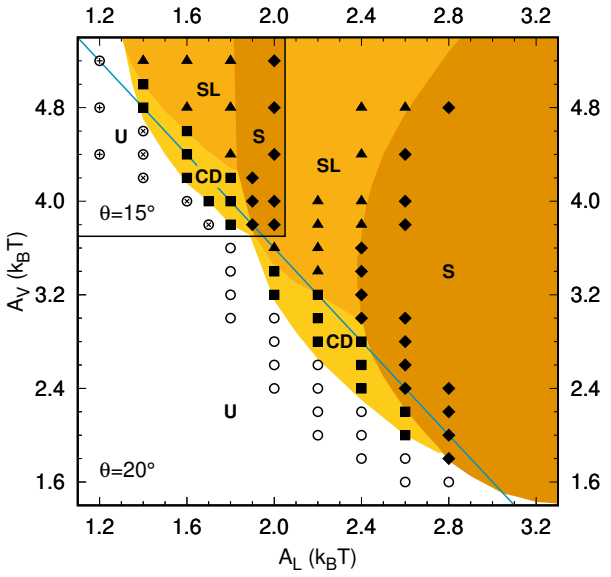

Fig. 4 GDP-MT behaviors as a function of vertical (A_V) and lateral (A_L) attraction strengths for $r_c = 0.75\sigma$ and $\theta = 20°$ (main) or $15°$ (inset). Symbols, labels, colors, and lines are the same as in Fig. 3.

$\Delta H_D^{max} \approx 30 k_B T$, with *diverse ratios* of lateral to vertical strengths that meet this criteria. First, the window in θ where catastrophic depolymerization occurs spans a range of approximately $\Delta\theta \sim 10°$: too low (e.g., $\theta < 10°$) and the GDP-MTs are not meaningfully destabilized, though binding is technically frustrated; too high (e.g., $\theta \approx 20°$) and the lattices are mechanically unstable unless attractions strengths are very high. Within the workable range of $\Delta\theta$, Fig. 3 also suggests there is a θ^* for which the footprint of catastrophic depolymerization is maximized (for $r_c = 0.50\sigma$, $\theta^* \approx 15°$). Meanwhile, the envelope of catastrophic depolymerization for a given θ spans combined lateral and vertical binding enthalpies ranging from $29 \leq \Delta H_D^{max} \leq 32 k_B T$. Interestingly, however, we observe that this ΔH_D^{max} can be variously apportioned between the lateral and vertical directions: for example, if we trace the boundary where $\Delta H_D^{max} = 30.4 k_B T$ (left and middle panels), we can find combinations of A_L and A_V that are laterally-biased ($\theta = 15°$, $A_{L,V} = 2.6, 2.4 k_B T$); roughly balanced ($\theta = 15°$, $A_{L,V} = 2.0, 3.6 k_B T$); or vertically-biased ($\theta = 10°$, $A_{L,V} = 1.4, 4.8 k_B T$) in terms of lateral versus vertical contributions to ΔH_D^{max}.

Fig. 4 shows the structural dynamics observed for $r_c = 0.75\sigma$ and two θ-values, where comparison with Fig. 3 reveals that the size and attributes of the catastrophic depolymerization manifold are robust to changes in r_c. In particular, by adopting the compression angles $\theta = 20°$ and $\theta = 15°$ for $r_c = 0.75\sigma$, we observe structural dynamics very comparable to those at $\theta = 15°$ and $\theta = 10°$ for $r_c = 0.50\sigma$. Here, of course, we have increased the θ values under examination, justified by the idea that because we have made the attraction ranges larger, we likewise must increase the degree of geometric frustration to generate comparable strain. But as before, all catastrophic depolymerization responses lie near the boundary of GDP-MT lattice and/or cap stability where $\Delta H_D^{max} \approx 30 k_B T$. Likewise, the behaviors at these two θ-values again point to a total range for depolymerization spanning $\Delta\theta \sim 10°$ (with, e.g., $\theta^* \approx 20°$). Of course, the robustness of the manifold properties cannot remain given *arbitrary* choices in r_c: certainly, as one shrinks r_c toward zero, GDP-MTs must become increasingly brittle, which would lead to instability (i.e., *any* geometric frustration is enough to cause lattice splits); in turn, if $r_c > 1\sigma$, one can imagine the current coarse-grained model cannot accommodate the geometric frustration required to generate strain (i.e., the attraction sites between vertical neighbors cannot be shifted sufficiently out of register). However, for any choices of r_c that qualitatively reflect the size of tubulin binding regions relative to the size of the tubulin subunits (our binding regions cover 8–13% of the subunit surface area and resemble the footprints of lateral binding regions[17]), the manifold of catastrophic depolymerization conditions appears predictably located within

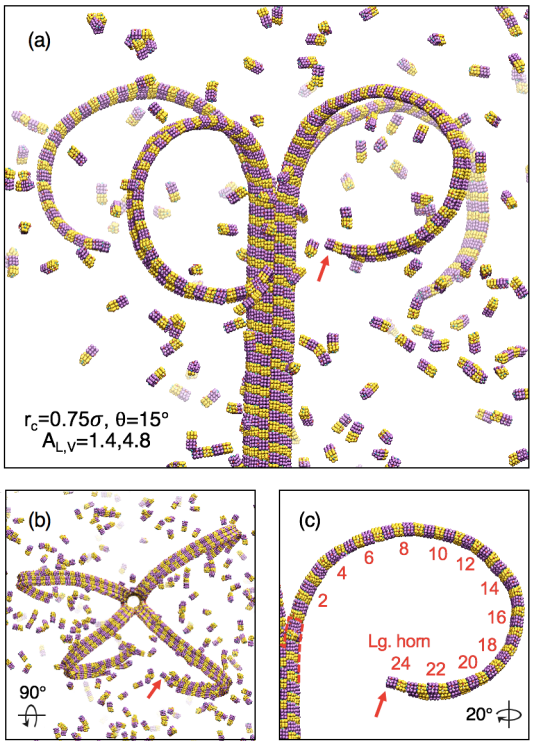

Fig. 5 MD snapshots of catastrophic depolymerization for an uncapped GDP-MT ($r_c = 0.75\sigma$, $\theta = 15°$, A_L=1.4k_BT, A_V=4.8k_BT) initially 320 dimers long (i.e., approx. 1.4μm). (a,b) Front and top views, respectively, of ram's horns observed at elapsed simulation time $\Delta t = 7.5x10^6\tau$. Red arrows indicate end of the ram's horn examined in (c). (c) Side view of largest ram's horn within configuration shown in (a,b), where dissociated dimers and other ram's horns have been removed for clarity. Numbers indicate the cumulative length (in dimers) of this ram's horn, starting from the terminal intact portion of the MT lattice (red dashed line). Rotations listed in (b,c) are relative to the view in (a).

the 4-dimensional parameter space of r_c, θ, A_L, and A_V.

The main distinguishing effect of different parameter sets upon catastrophic depolymerization is shown in Fig. 5, which shows simulation snapshots for $r_c = 0.75\sigma$ and vertically-biased attractions. (A movie of depolymerization at these conditions is provided in the ESI.) When compared with the snapshots in Fig. 2 (for $r_c = 0.50\sigma$ and laterally-biased attractions), these snapshots exhibit a more general observation: the unpeeling mechanism of catastrophic depolymerization is conserved across the manifold and the main effect is the alteration of the size of the ram's horns. The conserved attributes of the mechanism are as follows: (1) we always observe three to four ram's horns that each comprise three to four contiguous protofilaments at their base (i.e., three to four cracks in the lattice are necessary to relieve stress); (2) these ram's horns can be symmetrical (cf. Fig. 5) or, less frequently, asymmetrical in length and positioning (cf. Fig. 2); (3) occasionally during depolymerization, the boundaries of the ram's horns will shift horizontally and thus the ram's horns will comprise new distinguishable sets of protofilaments; and (4) ram's horns generally release dimers from their ends in ones or twos, and only very rarely will release whole sections of dimers or, e.g., break off of the tubule. On the other hand, ram's horns can vary from just a few dimers in length up to dozens of dimers in length, depending on the choice of parameters (discussed below). While the ram's horns in Fig. 2 are relatively short (6–8 dimers in length), the ram's horns shown in Fig. 5 are representative of the largest lengths we observed (25–30 dimers in length), where their completion of a revolution is similar to many of the ram's horns observed via cryo-EM[4,8].

Table 1 summarizes the effects of moving across the manifold in terms of persistence length, rate of depolymerization, and typical length of ram's horns for four "flagship" parameter sets that have the same $\Delta H_D^{max} = 30.4k_BT$. First, we highlight that these diverse parameters sets all generate highly-stiff model MTs, though the different attraction ranges and lateral/vertical strengths modulate stiffness. By calculating fluctuations in deflections of tethered GTP-MTs (capped GDP-MTs), we find model persistence lengths of $280 \leq \ell_p \leq 630\mu$m ($200 \leq \ell_p \leq 570\mu$m), which are comparable to experimental measurements made for short (< 500nm) Taxol-stabilized MTs[39,40]. In turn, we find that keeping attraction strengths constant, moving from $r_c = 0.50\sigma$ to $r_c = 0.75\sigma$ roughly halves the persistence lengths of GTP-MTs, a reflection of how the increased ability of individual subunits to locally "rattle" while maintaining bonds can collectively allow GTP-MTs to bend and twist to a greater degree. (Likewise, the persistence lengths of capped GDP-MTs decrease by about 40% with increasing r_c and commensurate increases in θ.) Secondly, we find that stronger vertical attractions result not only in stiffer GTP-MTs, but also result in smaller *losses* in stiffness (as low as 10%) when moving from GTP-MTs to capped GTP-MTs with the same attraction strengths. These effects are both sensible given that relatively stronger vertical binding would keep subunits in tighter register—particularly after hydrolysis causes subunit compression, where vertically-biased interactions generate more axial strain along the lattice and thus suppress local dimer rattling.

Table 1 also reveals how properties like depolymerization rate and sizes of ram's horns depend upon the length scales and relative strengths of lateral versus vertical binding. First, we note that given constant r_c and ΔH_D^{max}, there is little dependence of depolymerization rate on the relative balance of lateral versus vertical attractions. This is possible because dimers are mainly lost from the *exposed corners* at the ends of ram's horns, and thus what matters from an enthalpic perspective is the *total* binding energy from one lateral and one vertical neighbor. However, the depolymerization rate decreases by approximately 60% in going from $r_c = 0.50\sigma$ to $r_c = 0.75\sigma$— a trend that is expected as neighboring dimers must make more attempts to escape their attractive wells when those wells are larger, thus slowing dimer dissociation. As diagrammed in Fig. 5, we also calculate average lengths of the ram's horns (based on the instantaneously longest ram's horn, defined as the exposed portion of protofilaments beyond the depolymerization front) and find that ram's horns are longer when dimer binding attractions are vertically biased. This is sensible as relatively stronger vertical interactions would tend to generate greater axial stress along the lattice that can only be dissipated through additional outward curling of the protofilaments. Ram's horns are also longer given larger r_c values— a secondary effect of the trend discussed above where the escape rate is decreased

Table 1 MT properties for various catastrophic depolymerization (CD) conditions, including maximum enthalpy changes $\Delta H_{L,D}^{max}$ ($\Delta H_{V,D}^{max}$) for dimer-dimer binding in lateral (vertical) directions; persistence lengths L_p (in equivalent μm) for GTP-MTs populated with uncompressed dimers and capped GDP-MTs, respectively; and CD rates and corresponding length scales of ram's horns (specifically longest exposed protofilaments, see Fig. 5) for uncapped GDP-MTs.

CD conditions ($\Delta H_D^{max} = 30.4 k_B T$)						GTP-MT	GDP-MT (cap)	GDP-MT (no cap)	
r_{cut}	θ	A_L	A_V	$\Delta H_{L,D}^{max}$	$\Delta H_{V,D}^{max}$	L_p (μm)	L_p (μm)	CD rate (rows/$10^5\tau$)	Lg. horn (no. dimers)
0.50	10°	1.4	4.8	-11.2	-19.2	630.0	573.1	1.98 ± 0.0643	12.9 ± 2.65
0.50	15°	2.2	3.2	-17.6	-12.8	531.7	291.2	1.84 ± 0.171	6.24 ± 1.59
0.75	15°	1.4	4.8	-11.2	-19.2	380.2	343.2	0.765 ± 0.102	28.5 ± 3.91
0.75	20°	2.2	3.2	-17.6	-12.8	283.5	198.1	0.754 ± 0.0681	9.18 ± 1.98

by larger r_c. This occurs because the steady-state lengths of ram's horns are based on the corresponding kinetic balance between propagation of the unpeeling front and ease of dimer dissociation during the initiation (i.e., transient start-up) of depolymerization.

3.2 Interruption of catastrophic depolymerization

We next consider whether catastrophic depolymerization of the model GDP-MTs can be interrupted by the presence of small regions of uncompressed dimers (i.e., GTP-rich regions) resembling so-called "GTP remnants" thought to initiate MT rescue in experiments.[31] As shown in Figs. 6(a) and 6(k), we incorporate uncompressed dimers into "interruption regions" within the lattices of uncapped GDP-MTs that are 160 dimers long (1.4 μm). These regions comprise two or four rows of dimers, where we replace a number of the compressed dimers per row with uncompressed dimers. (Notation-wise, we label these regions by number of rows and number of uncompressed dimers per row, so a two-row region with four uncompressed dimers per row is an "r2p4" region.) We then perform MD simulations where we allow catastrophic depolymerization to initiate and observe whether it is interrupted (i.e., arrested) when the unpeeling front approaches the interruption region and how long it takes for depolymerization to reinitiate. Here, we do not supply additional GTP-tubulin and reserve an analysis of rescue itself for future reports.

As illustrated in Fig. 6, even small interruption regions can indeed interrupt depolymerization in-progress, frustrating the propagation of the unpeeling front. (An additional movie of interruption is shown in ESI.) The duration of the interruption depends on the composition and placement of the uncompressed dimers. As shown in Fig. 7, we can quantify these time scales of interruption by looking at the trace of MT length over time, selecting the portions where the tubule length is approximately constant and corresponds to the interruption region. By repeating this process for 10 different uncapped GDP-MTs with randomly-generated interruption regions (i.e., fixing the number of rows and desired occupancy, but randomly assigning the uncompressed dimer positions), we get a sense for the variable time scales of successful interruption. As illustrated in Fig. 7, we also determine the cluster geometries of the uncompressed dimers that are more successful at interrupting depolymerization. In particular, we observe that evenly-distributed dimers that leave "lanes" for the ram's horns to cut through have short interruption times. In contrast, larger interruption times are seen when uncompressed dimers are organized into what resemble small partial stabilizing caps.

In Fig. 8, we show results of the time-scale analysis above for two different combinations of r_c, θ, A_L, and A_V (cf. Table 1) and interruption regions of different sizes and occupancies. In all cases, it is clear that interruption regions containing only a dozen or more dimers are sufficient to interrupt depolymerization at least temporarily, and thus that the presence of uncompressed dimers as a potential point of MT rescue is a generic feature of conditions where catastrophic depolymerization occurs. In turn, we consistently observe that the greater the number of rows in the interruption region, the longer the average interruption time. Interestingly, we also find the average interruption time increases *exponentially* based on the number of uncompressed dimers per row X (or, alternatively, per region), where the average interruption time Δt_{int} normalized by the average time for dimer row loss Δt_{row} during depolymerization is given by

$$\langle \Delta t_{int} \rangle / \langle \Delta t_{row} \rangle = t_0 \exp(kX) \quad (2)$$

where t_0 and k are constants. Crucially, the exponential nature of the curves in Fig. 8 supports the idea that average interruption times are predictable, which is lent further credence as the average interruption times for the two-row r2pX and four-row r4pX interruption regions (at $r_c = 0.50\sigma$) collapse roughly onto one another when plotted based on the *total number* of uncompressed dimers present (not shown).

Finally, Fig. 8 underlines how sensitive catastrophic depolymerization is to incomplete hydrolysis: interruption regions need only comprise two or three dozen uncompressed dimers in a matter of a few dimer rows to generate interruption times *orders of magnitude* longer than the time scales of MT depolymerization, and thus to serve as potential points for rescue. Typical experimental estimates for MT depolymerization rate place the loss of dimer rows at up to 30 to 50 times faster than typical dimer row addition rate during growth; thus, for potential rescue, one would conservatively want to stabilize an otherwise depolymerizing MT for at least 100 times the rate of dimer row loss. This would then account for (1) the time during which ram's horns are exhausted, so that newly added GTP-tubulin can form a contiguous cap; and (2) the time for addition of a full stabilizing row (or more) of GTP-tubulin. The results in Fig. 8 indicate that such a 100-fold stabilization can be achieved (in four-row cases) for 5 dimers per row (r4p5) for the $r_c = 0.50\sigma$ case and 9 dimers per row (r4p9) for the $r_c = 0.75\sigma$ case— i.e., given approximately 20 to 36 dimers in the span of a few dimer rows. Here, the $r_c = 0.75\sigma$ case would tend to represent one of the hardest systems to inter-

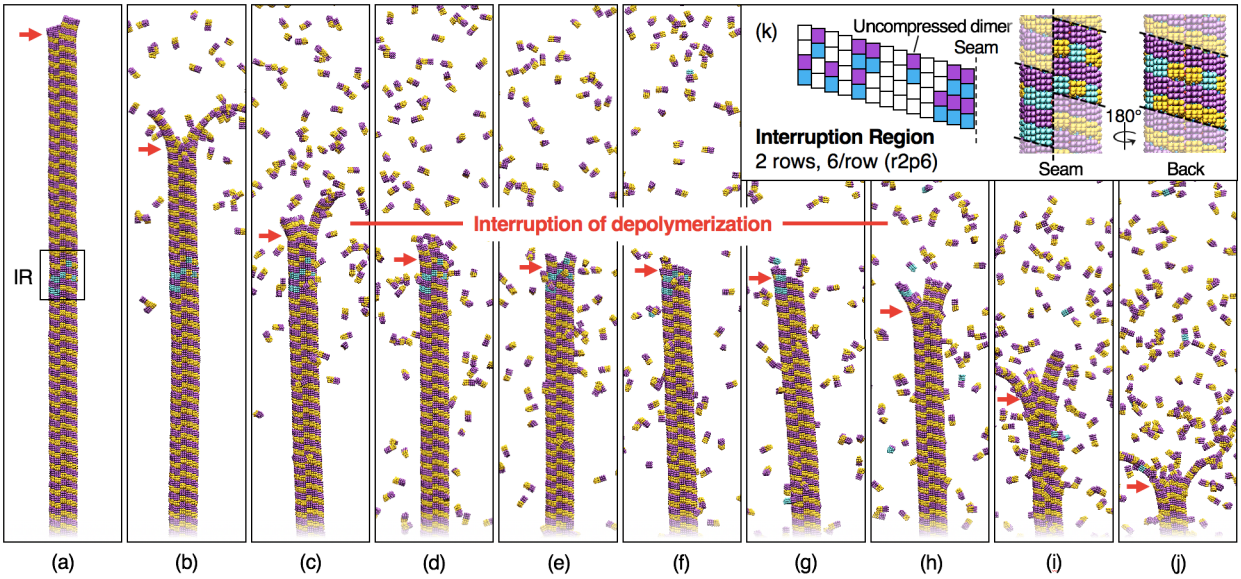

Fig. 6 (a-j) Time-lapse series of snapshots (increments of $\Delta t = 0.4\text{x}10^6\tau$) showing interruption of catastrophic depolymerization for an uncapped GDP-MT ($r_c = 0.50\sigma$, $\theta = 15°$, A_L=2.2k_BT, A_V=3.2k_BT) with a randomly-generated interruption region spanning 2 rows that each contain 6 uncompressed dimers (r2p6). The box in panel (a) indicates the interruption region (IR) detailed in (k) and the red arrows in panels (a-j) denote the farthest intact row. (k) Diagram representation of the r2p6 interruption region (left) and corresponding initial snapshots of the MT lattice (right), where the 2-row region corresponding to the diagram is highlighted and traced by dotted lines.

rupt within the parameter manifold given its aggressive unpeeling mechanism due to vertically-biased interactions. Nevertheless, just as it is understood that very minimal caps serve to stabilize MTs in experiments (and as small as 1 to 2 rows are sufficient to stabilize model GDP-MTs), it is clear that only 2 to 4 partially unhydrolyzed rows may be sufficient to interrupt even aggressive depolymerization in-progress.

4 Conclusions

We have used molecular dynamics simulations of a coarse-grained tubulin model to reveal the manifold in parameter space where the balance between tubulin binding interactions and tubulin shape change (i.e., α-subunit compression) yields dynamic instability in MTs. Specifically, we have discovered the conditions–with respect to the length scales of binding attractions (r_c), the degree of subunit compression (θ), and the strengths of lateral and vertical attractions (A_L and A_V)— under which GTP-MTs are stable and otherwise highly-stiff GDP-MTs undergo catastrophic depolymerization when uncapped. In turn, we have found that this manifold of catastrophic depolymerization conditions spans approximately $10° \leq \theta \leq 20°$ for reasonable choices of r_c, and corresponds with total dimer binding enthalpies $29 \leq \Delta H_D^{max} \leq 32 k_B T$. Notably, however, we have seen that *diverse ratios* of lateral and vertical binding energies corresponding to these totals can facilitate catastrophic depolymerization, ranging from conditions where lateral interactions are dominant, lateral and vertical interactions are roughly balanced, or vertical interactions are dominant. Thus, more diversity is possible than found in biological MTs, which are understood to exhibit vertically-biased interactions.[25,28,41]

While the overall mechanism of catastrophic depolymerization is conserved across diverse parameter sets, we have also revealed how moving across the manifold of parameters affects (or does not) tubule stiffness, depolymerization rate, and lengths of ram's horns. For four select parameter sets spanning the manifold, all GTP-MTs and GDP-MTs are highly-stiff (with persistence lengths comparable to those measured in experiments), where smaller attraction length scales and more vertically-biased attractions result in stiffer tubules and less losses in stiffness when switching from GTP- to GDP-MTs. Depolymerization rates are not sensitive to the lateral- or vertical-bias of attractions as dimer dissociation is mainly dependent on total ΔH_D^{max}, but are sensitive to the choice of r_c, which sets the rate of dimer dissociation and thus affects the steady-state progress of depolymerization. In contrast, the lengths of ram's horns are sensitive to both the balance and length scale of attractions: more vertically-biased attractions and larger r_c both tend to result in larger ram's horns as they move the kinetic balance between propagation of the unpeeling front and dimer dissociation toward propagation during start-up (which then sets the steady-state length). The largest ram's horns we have observed in detail— at $r_c = 0.75\sigma$, $\theta = 15°$, $A_{L,V} = 1.4, 4.8 k_B T$— are approximately 25-30 dimers in length, similar to many ram's horns observed via cryo-EM.[4,8]

Finally, we have demonstrated that small GDP-MT lattice regions containing uncompressed dimers can interrupt depolymerization in-progress for timescales that would facilitate rescue, echoing the picture of "GTP remnants" (i.e., clusters of GTP-tubulin) found in experiments to serve as locations for rescue initiation. By measuring average interruption times for interruption regions of various sizes (number of dimer rows) and compositions (number of uncompressed dimers per row), we have observed that the effectiveness of these interruption regions in terms of time interrupted is predictable and exponential on average with respect to the number of uncompressed dimers. How-

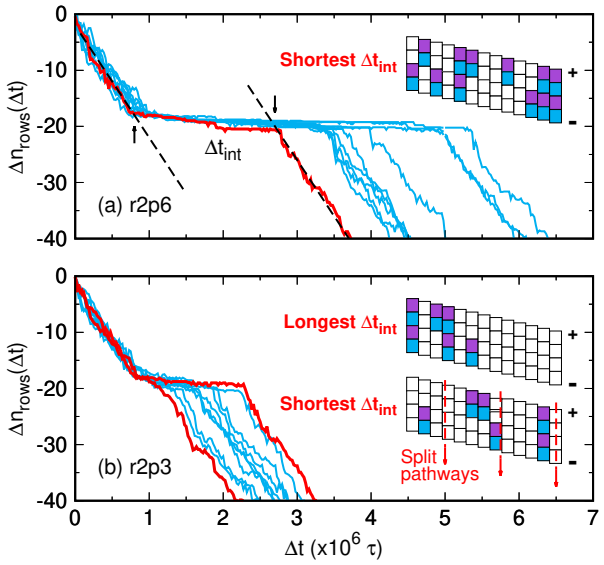

Fig. 7 Net loss of intact MT lattice dimer rows $\Delta n_{\text{rows}}(\Delta t)$ versus elapsed simulation time Δt for 10 independent simulations of uncapped GDP-MTs ($r_c = 0.50\sigma$, $\theta = 15°$, A_L=2.2k_BT, A_V=3.2k_BT) with randomly-generated interruption regions spanning 2 rows that each contain (a) 6 uncompressed dimers (r2p6) or (b) 3 uncompressed dimers (r2p3). In (a), dashed lines indicate progression of catastrophic depolymerization for one highlighted case (thick red line), where the time elapsed between these fit lines corresponds to the interruption timescale Δt_{int}. Diagrams in (a,b) show positions of the uncompressed dimers in the interruption regions corresponding to the cases highlighted by thick red lines. Plus and minus signs indicate direction of microtubule axis. For the shortest interruption time in (b) where $\Delta t_{\text{int}} \approx 0\tau$, arrows in the rightward diagram indicate crack pathways between three depolymerizing ram's horns (each spanning 4 contiguous protofilaments) that propagate through the interruption region.

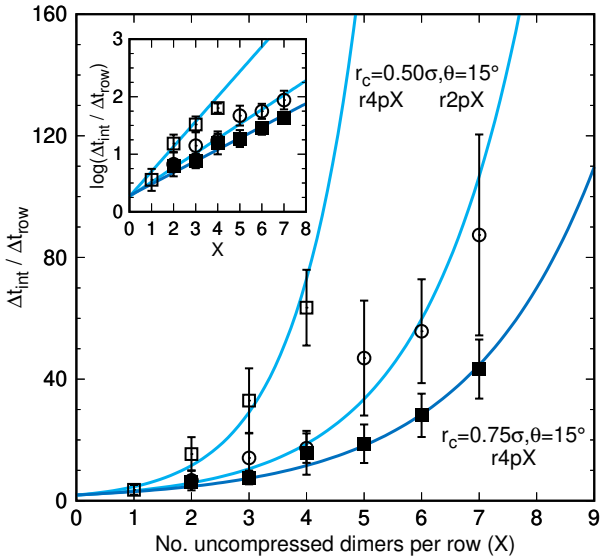

Fig. 8 Averages and standard deviations of interruption times Δt_{int} normalized by the times for loss of one dimer row during depolymerization Δt_{row} (i.e., inverse of CD rates, cf. Table 1) versus number of uncompressed dimers per row (X) of interruption regions for three different uncapped GDP-MT systems: CD conditions $r_c = 0.50\sigma$, $\theta = 15°$, A_L=2.2k_BT, A_V=3.2k_BT with 2-row (r2pX, unfilled diamonds) or 4-row (r4pX, unfilled squares) interruption regions and CD conditions $r_c = 0.75\sigma$, $\theta = 15°$, A_L=1.4k_BT, A_V=4.8k_BT with 4-row (r4pX, filled squares) interruption regions. Solid blue lines show fits to the average normalized interruption times using Eq. (2). For the $r_c = 0.50\sigma$ conditions, $t_0 = 1.84$ and $k = 0.92$ and 0.58 for the r4pX and r2pX interruption regions, respectively. For the $r_c = 0.75\sigma$ conditions and r4pX regions, $t_0 = 1.91$ and $k = 0.45$. Inset shows the same normalized interruption times plotted on log-basis.

ever, interruption regions are most successful when several uncompressed dimers are configured into a small connected cluster. In turn, as few as two to three dozen uncompressed dimers, if all located within a few lattice rows, are sufficient to generate interruption times *orders of magnitude* longer than the time scales of MT depolymerization— essentially acting as a new minimal cap for initiating MT growth. Taken altogether, these results again underline how tubulin subunit shape is a driving force not only for initiating catastrophic depolymerization but also for interrupting (and reversing) it.

Looking forward, the coarse-grained model for tubulin used here will not only facilitate further micro-mechanical studies of MT behavior, but also represents a promising blueprint for the realization of synthetic responsive MTs. In future reports, we will examine the nucleation and growth mechanisms of this model across the manifold of catastrophic depolymerization conditions, considering in detail the thermodynamic and kinetic consequences of the interplay between tubulin binding interactions and subunit shape change. Meanwhile, the patchy wedges examined here have effectively been synthesized via DNA-origami techniques and shown to reversibly form micron-scale tubules (though presently without accompanying shape change capability).[10] We anticipate that given the shape change deployed here to drive the dynamic instability resembles a deformation accomplishable via modest unidirectional actuation, an analogous stimuli-induced (e.g., pH, temperature, co-solute) compression[42] of synthetic wedges can result in similarly responsive tubules or fibers. This will no doubt serve as another route to understand how subunit shape change underlies the rich structural-dynamic properties of MTs.

Acknowledgements

This research was supported by the U.S. Department of Energy, Office of Basic Energy Sciences, Division of Materials Sciences and Engineering under Award KC0203010. This work was performed, in part, at the Center for Integrated Nanotechnologies, an Office of Science User Facility operated for the U.S. Department of Energy (DOE) Office of Science. Sandia National Laboratories is a multi-mission laboratory managed and operated by National Technology and Engineering Solutions of Sandia, LLC., a wholly owned subsidiary of Honeywell International, Inc., for the U.S. Department of Energy's National Nuclear Security Administration under contract DE-NA0003525. This paper describes objective technical results and analysis. Any subjective views or opinions that might be expressed in the paper do not necessarily represent the views of the U.S. Department of Energy or the United States Government.

Conflict of interest

There are no conflicts to declare.

References

1 T. Mitchison and M. Kirschner, *Nature*, 1984, **312**, 237–242.
2 A. Desai and T. J. Mitchison, *Annu. Rev. Cell Dev. Biol.*, 1997, **13**, 83–117.
3 S. Maurer, F. Fourniol, G. Bohner, C. Moores and T. Surrey, *Cell*, 2012, **149**, 371 – 382.
4 E. M. Mandelkow, E. Mandelkow and R. A. Milligan, *J. Cell Biol.*, 1991, **114**, 977–991.
5 D. Chrétien, S. D. Fuller and E. Karsenti, *J. Cell Biol.*, 1995, **129**, 1311–1328.
6 J. Howard and A. Hyman, *Nature*, 2003, **422**, 753–758.
7 S. Westermann, H.-W. Wang, A. Avila-Sakar, D. G. Drubin, E. Nogales and G. Barnes, *Nature*, 2006, **440**, 565–569.
8 H. Y. Kueh and T. J. Mitchison, *Science*, 2009, **325**, 960–963.
9 M. A. Jordan and L. Wilson, *Nat. Rev. Cancer*, 2004, **4**, 253–265.
10 K. F. Wagenbauer, C. Sigl and H. Dietz, *Nature*, 2017, **552**, 78–83.
11 J. Boekhoven, W. E. Hendriksen, G. J. M. Koper, R. Eelkema and J. H. van Esch, *Science*, 2015, **349**, 1075–1079.
12 K.-T. Wu, J. B. Hishamunda, D. T. N. Chen, S. J. DeCamp, Y.-W. Chang, A. Fernández-Nieves, S. Fraden and Z. Dogic, *Science*, 2017, **355**, year.
13 T. Müller-Reichert, D. Chrétien, F. Severin and A. A. Hyman, *Proc. Natl. Acad. Sci. U. S. A.*, 1998, **95**, 3661–3666.
14 E. Nogales, S. G. Wolf and K. H. Downing, *Nature*, 1999, **391**, 199–203.
15 E. A. Geyer, A. Burns, B. A. Lalonde, X. Ye, F.-A. Piedra, T. C. Huffaker and L. M. Rice, *eLife*, 2015, **4**, e10113.
16 G. M. Alushin, G. C. Lander, E. H. Kellogg, R. Zhang, D. Baker and E. Nogales, *Cell*, 2014, **157**, 1117 – 1129.
17 R. Zhang, G. M. Alushin, A. Brown and E. Nogales, *Cell*, 2015, **162**, 849 – 859.
18 R. B. Ravelli, B. Gigant, P. A. Curmi, I. Jourdain, S. Lachkar, A. Sobel and M. Knossow, *Nature*, 2004, **428**, 198–202.
19 H.-W. Wang and E. Nogales, *Nature*, 2005, **435**, 911–915.
20 I. M. Jánosi, D. Chrétien and H. Flyvbjerg, *Biophys. J.*, 2002, **83**, 1317 – 1330.
21 V. VanBuren, D. J. Odde and L. Cassimeris, *Proc. Natl. Acad. Sci. U. S. A.*, 2002, **99**, 6035–6040.
22 E. B. Stukalin and A. B. Kolomeisky, *J. Chem. Phys.*, 2004, **121**, 1097–1104.
23 M. I. Molodtsov, E. A. Ermakova, E. E. Shnol, E. L. Grishchuk, J. R. McIntosh and F. I. Ataullakhanov, *Biophys. J.*, 2005, **88**, 3167–3179.
24 V. VanBuren, L. Cassimeris and D. J. Odde, *Biophys. J.*, 2005, **89**, 2911 – 2926.
25 M. K. Gardner, B. D. Charlebois, I. M. Jánosi, J. Howard, A. J. Hunt and D. J. Odde, *Cell*, 2011, **146**, 582–592.
26 G. Margolin, I. V. Gregoretti, T. M. Cickovski, C. Li, W. Shi, M. S. Alber and H. V. Goodson, *Mol. Biol. Cell*, 2012, **23**, 642–656.
27 X. Li and A. B. Kolomeisky, *J. Phys. Chem. B*, 2014, **118**, 13777–13784.
28 P. Zakharov, N. Gudimchuk, V. Voevodin, A. Tikhonravov, F. I. Ataullakhanov and E. L. Grishchuk, *Biophys. J.*, 2015, **109**, 2574–2591.
29 J. A. Bollinger and M. J. Stevens, *Soft Matter*, 2018, **14**, 1748–1752.
30 M. Caplow and J. Shanks, *Mol. Biol. Cell*, 1996, **7**, 663–675.
31 A. Dimitrov, M. Quesnoit, S. Moutel, I. Cantaloube, C. Poüs and F. Perez, *Science*, 2008, **322**, 1353–1356.
32 C. Tropini, E. A. Roth, M. Zanic, M. K. Gardner and J. Howard, *PLoS One*, 2012, **7**, 1–5.
33 M. K. Gardner, M. Zanic and J. Howard, *Curr. Opin. Cell Biol.*, 2013, **25**, 14 – 22.
34 C. Aumeier, L. Schaedel, J. Gaillard, K. John, L. Blanchoin and M. Théry, *Nat. Cell Biol.*, 2016, **18**, 1054–1064.
35 C. P. Fees and J. K. Moore, *Mol. Biol. Cell*, 2019, **30**, 753–765.
36 S. Cheng, A. Aggarwal and M. J. Stevens, *Soft Matter*, 2012, **8**, 5666–5678.
37 S. Cheng and M. J. Stevens, *Soft Matter*, 2014, **10**, 510–518.
38 S. Plimpton, *J. Comput. Phys.*, 1995, **117**, 1 – 19.
39 F. Pampaloni, G. Lattanzi, A. Jonáš, T. Surrey, E. Frey and E.-L. Florin, *Proc. Natl. Acad. Sci. U. S. A.*, 2006, **103**, 10248–10253.
40 K. M. Taute, F. Pampaloni, E. Frey and E.-L. Florin, *Phys. Rev. Lett.*, 2008, **100**, 028102.
41 O. Kononova, Y. Kholodov, K. E. Theisen, K. A. Marx, R. I. Dima, F. I. Ataullakhanov, E. L. Grishchuk and V. Barsegov, *J. Am. Chem. Soc.*, 2014, **136**, 17036–17045.
42 A. Cangialosi, C. Yoon, J. Liu, Q. Huang, J. Guo, T. D. Nguyen, D. H. Gracias and R. Schulman, *Science*, 2017, **357**, 1126–1130.

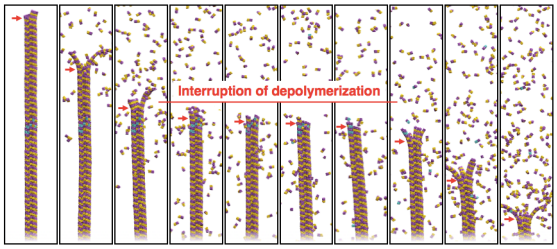

Figure 1: Microtubules undergo catastrophically-fast depolymerization that can be reversed during "rescue" events. Coarse-grained molecular simulations reveal how these behaviors may be controlled tubulin conformation.